*Energy Storage and Conversion* 2024, 2(4), 562.
https://doi.org/10.59400/esc.v2i4.562

Article

# Tailored copper doped indium sulfide nanostructures as electrode material for supercapacitor and nano photocatalyst for dye degradation

**K.Lilly Mary[1,*], D. Geetha[1,*], P.S. Ramesh[2]**

[1] Department of Physics, Annamalai University, Chidambaram, Tamil Nadu 608002, India
[2] Thiru Kolanjiappar Government Arts College, Virudhachalam, Tamil Nadu 606001, India
*** Corresponding authors:** Lilly Mary K., lillyjoy1305@gmail.com; Geetha D., geeramphyau@gmail.com

**CITATION**

Mary KL, Geetha D, Ramesh PS. Tailored copper doped indium sulfide nanostructures as electrode material for supercapacitor and nano photocatalyst for dye degradation. Energy Storage and Conversion. 2024; 2(4): 562. https://doi.org/10.59400/esc.v2i4.562

**ARTICLE INFO**

Received: 21 February 2024
Accepted: 18 September 2024
Available online: 3 October 2024



**Abstract:** The unique copper-doped indium sulfide nanocrystals are synthesized by a gentle hydrothermal process. XRD, FTIR, XPS, FESEM/EDX, UV-DRS, and PL were used to characterize the final samples. Copper-doped indium sulfide nanostructures can be exploited as an active catalyst in photodegradation and as an electroactive material in supercapacitors due to their distinctive architecture. The copper-doped indium sulfide catalyst exhibits 85 percent photodegradation using methylene blue dye under natural sunlight irradiation, and the electrochemical test showed a capacitance of 668 $Fg^{-1}$ at 1 $Ag^{-1}$ in a 2 M KOH electrolyte solution. For future generations, photocatalyst and electrode can function as more desirable materials.

**Keywords:** copper-doped indium sulfide; supercapacitors; methylene blue; photodegradation

## 1. Introduction

Nano-sized semiconducting materials are great interest in materials research due to their size- and shape-dependent optical, electrical, and catalytic characteristics. In particular, Cadmium and lead chalcogenides have been the topic of extensive investigation during the last 20 years [1,2]. Despite their fascinating properties, the toxicity of cadmium and lead limits their potential for widespread application. As a result, tertiary and quaternary materials such as semiconductors based on copper, indium, zinc, and tin scientific interest as potential alternatives. Indium sulfide, a major group III-VI semiconductor, has shown potential for solar applications, band gap energy (2.0–2.4 eV), excellent transparency photoconductive behaviour. Energy and environmental crises are the most pressing issues of the twenty-first century, and indium sulfide, an n-type semiconductor that had most stability at room temperature, is being investigated as a potential photoconductive material as replacement material for hazardous CdS [3,4]. As a result, photocatalytic technology is a desired way for generating renewable energy and cleaning up the environment [5–7]. Photocatalytic water splitting is a successful approach for producing solar hydrogen [8–10]. Several photocatalysts have been thoroughly researched up to this point for both pollutant oxidation and hydrogen production.

The indium sulfide photocatalyst is a viable option among photocatalytic materials with advantageous properties that can be used in a variety of environmental and energy applications. Only one review study in the Journal of Photochemistry and Photobiology [11] discusses indium sulfide as a photocatalyst for solar energy conservation. The Scopus database was searched over the last ten years to assess the most recent works on indium sulfide as a photocatalyst. It was observed that indium

sulfide is a potent catalyst for numerous photocatalytic purposes.

In view of the growing need for electric energy especially the portable consumer electronics and hybrid electric vehicles, there has been a worldwide interest in developing new type of electrode materials [12]. In terms of power density is higher than previous electrode, quick charge-discharge process, and extended lifespan, supercapacitors and ultracapacitors are emerging as a new force in the field of energy storage devices. The charge storage mechanism is mostly awaited in energy storage, supercapacitors are classified into two types: electrical double-layer capacitors controlled by the charge of electrostatic forces separates in the electrode/electrolyte interface and pseudo capacitors controlled at the electrode interface by faradic processes [13]. Supercapacitors have several advantages over traditional electric storage devices, including the capacity to deliver up to 10 times the power of batteries, fast charging in seconds, and high long-cycle stability. These characteristics lend themselves to useful applications. The properties of the electrode materials employed in ultracapacitors have a significant impact on their capacitive performance [14]. Nano powders properties are improved by Doping of metal ions. The standard hydrothermal approach is employed in this study to produce both pure and Cu-doped InS nanoparticles. In addition to sol-gel processing, hydrothermal, co-precipitation, chemical vapor deposition, and microemulsion methods have been used to successfully manufacture indium sulfide nanoparticles. The hydrothermal approach is frequently used to create pure and doped nanoparticles (NPs) at room temperature and at a reasonable cost [15–17]. Cu-doped InS nanoparticles were synthesized using a simple hydrothermal approach for application in electrochemical and photocatalytic processes, and the effects of the dopants on the materials generated were investigated. The Cu (0.1) g-doped indium sulfide nano samples developed are suitable for use in energy storage applications.

## 2. Experimental approaches

### 2.1. Materials and methods

Indium chloride ($InCl_3$), thiourea $CS(NH_2)_2$, oxalic acid, ammonia, copper (II) chloride ($CuCl_2$) reagents were purchased from Sigma Aldrich and utilized without further purification

### 2.2. Copper-doped indium sulfide synthesis

To make a standardized solution, 25 mmol of indium chloride, 350 mmol of thiourea, and 25 mL of filtered water were mixed in a conical flask and constantly swirled. After 10 min, reducing and complexing agents, oxalic acid and ammonia, were added. Copper chloride ($CuCl_2$) was added in varying proportions to $InCl_3$ and CS $(NH_2)_2$ to make copper-doped indium sulfide. The next solution was kept into a Teflon-lined autoclave, sealed, and kept at 120 C for 5 h. To create nanoparticles, the sample was dried in a hot air oven at 80 ℃ for 5 h, followed by 1 h in a muffle furnace at 300 ℃. The autoclave was allowed to cool naturally to room temperature. The precipitate was centrifuged for separation, rinsed the precipitate with ethanol and distilled water in many times.

### 2.3. Characterization procedure

Using an X-ray diffractometer, the crystal size of copper-doped indium sulfide nano samples was determined to describe photoluminescence spectra obtained using a spectrophotometer excited between 400 and 800 nm. The morphology was observed with FE-SEM, and UV-DRS measurements in the 220–1400 nm range were performed with a diffuse reflectance spectrometer. X-ray photo electron spectroscopy (XPS), cyclic voltammetry (CV), galvanostatic charge—discharge (GCD), and electrochemical impedance (EIS) were used.

## 3. Result and discussion

### 3.1. Structural analysis (XRD)

XRD is used to analyze the crystalline structure of pure indium sulfide and copper-doped indium sulfide. **Figure 1a** shows pure indium sulfide, while **Figure 1b–d** show various amounts of copper-doped indium sulfide nanoparticles.

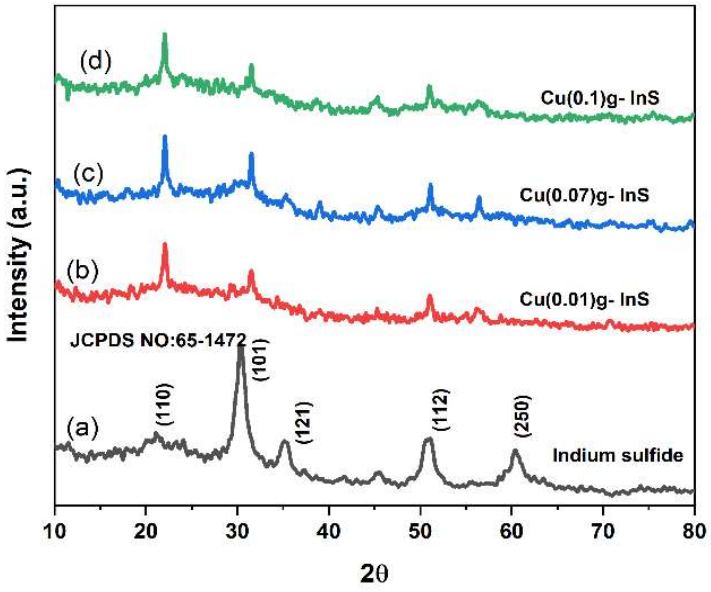


**Figure 1.** XRD pattern of synthesized. **(a)** Indium sulfide; **(b)** Cu (0.01) g; **(c)** Cu (0.07) g; **(d)** Cu (0.1) g doped Indium sulfide NPs.

According to the XRD pattern, the synthesized nanoparticles are polycrystalline and have an orthorhombic structure, which is consistent with the theoretical expectations (JCPDS No; 65–1472). The XRD pattern of copper-doped indium sulfide nanoparticles are remarkably identical to that of undoped indium sulfide nanoparticles since new phases were found and there was no structural change. The addition of (0.01) g of copper enhanced the peak intensity greatly in the XRD pattern of synthesized copper-doped indium sulfide. This could be attributed to an increase in the size of the crystalline structure [18,19].

The average size of a Crystallite could be calculated using the Debye—Scherer formula [20,21].

$$D = \frac{k\lambda}{\beta \cos\theta}$$

The calculated values, where $D$, and $k$ denote the crystallite size, incident radiation wavelength, geometrical factor (0.9), measured angle, and FWHM, respectively.

When the copper concentration was increased to 0.1 g, the crystallite sizes grew, and the lattice parameter of the generated nanoparticles was calculated using the following expression:

$$\frac{1}{d^2} = \frac{h^2}{a^2} + \frac{k^2}{b^2} + \frac{l^2}{c^2}$$

Interplanar spacing and miller indices are represented by $d$ and $h$, $k$, $l$, respectively. Doping occurs proved by the comparative study of radius of $Cu^{2+}$ (0.73 Å) is less than that of $In^{3+}$ (0.80 Å). The dislocation density and micro strain of copper-doped indium sulfide nanoparticles were calculated using the following equations [22–24].

$$\delta = \frac{1}{D^2}$$

$$\varepsilon = \beta \cos \theta/4$$

The dislocation density and micro strain of copper-doped indium sulfide nanoparticles were determined using the equations are in the **Table 1**.

**Table 1.** Structural parameters of pure InS and Cu-doped InS nanoparticles.

| Samples | Average Crystallite Size (nm) | Dislocation Density ($\delta$) (X 1015 M-2) | MicroStrain ($\varepsilon$) X 10-3 | Lattice Parameters (Å) | | |
|---|---|---|---|---|---|---|
| | | | | A | B | C |
| Indium Sulfide | 10 | 3.73 | 5.56 | 4.442 | 10.64 | 3.939 |
| Cu(0.01)g doped Ins | 14 | 3.54 | 5.10 | 3.939 | 4.442 | 10.50 |
| Cu(0.07)g doped Ins | 17 | 2.82 | 3.46 | 3.939 | 4.442 | 10.50 |
| Cu(0.1)g doped Ins | 20 | 2.37 | 2.50 | 3.939 | 4.442 | 10.50 |

## 3.2. Spectral analysis (FTIR)

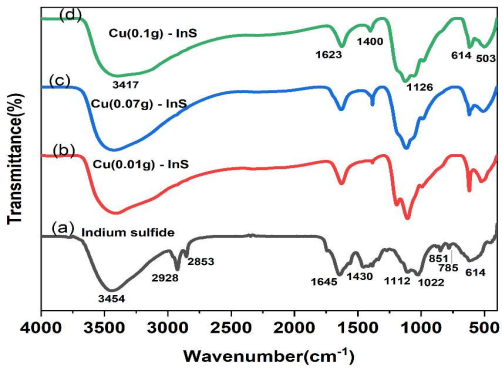


**Figure 2.** FTIR spectra of synthesized. **(a)** Indium sulfide; **(b–d)** Cu (0.01, 0.07, 0.1) g doped InS NPs.

The FTIR spectrum was shown in **Figure 2** to help comprehend the synthesis of indium sulfide nanoparticles and the numerous functional groups found in the samples. The **Figure 2** depicts an analysis of the FTIR spectrum from 4000 to 400 $cm^{-1}$ [25]. The optical band gap, surface form, and crystallite structure all have an effect on band locations and presence of the number of absorption peaks.

It is also in responsible of determining the material's elemental makeup. Broad absorption bands in all samples, with wavelengths ranging from 3550 to 3200 $cm^{-1}$, confirmed the presence of the O–H and the hydroxyl group of $H_2O$ molecules from stretching vibration absorbed on the surfaces [26,27]. The existence of absorbed compounds on the surfaces of pure nanocrystals is indicated by absorption peaks in between the range of 3000–2840 $cm^{-1}$, which correspond to specific symmetric and asymmetric C–H stretching mode groups reduced in the Cu-doped InS spectra. Because of the presence of organic compounds in the samples, absorption bands between 1600 and 1400 $cm^{-1}$ were observed, which correspond to the C = C stretching. The stretching modes of the In-S band may be responsible for the absorption peaks below 1000 $cm^{-1}$. S band stretching peaks are responsible for the absorption peak at 614 $cm^{-1}$ for pure indium sulfide (0.1) g. The FTIR and XRD patterns demonstrate the efficacy of doping indium sulfide with an impurity-free crystalline substance. Cu doping of 0.01 g, 0.07 g, and 0.1 g improved the In-S, Cu stretching absorption band at 614 $cm^{-1}$ and 503 $cm^{-1}$. The incorporation of Cu doped-InS lattice structure is shifted at little frequency in absorption band. As a result, these bands absorbed more FTIR wavelengths are extended than undoped InS nanoparticles. Infrared peaks with wavelengths less than 700 $cm^{-1}$ are ideal for analyzing InS bands and functional groupings [28].

## 3.3. Morphological analysis (FESEM /EDX)

FESEM micrographs of indium sulfide and copper doped indium sulfide nanocrystals (0.01 g, 0.07 g, 0.1 g) were recorded. Indium sulfide has an uneven spherical shape with particle agglomeration, as shown in **Figure 3a–d** depicts the spherical form of evenly distributed nanocrystals. The degree of agglomeration increases with doping concentration, as seen in the graph for copper-doped indium sulfide.

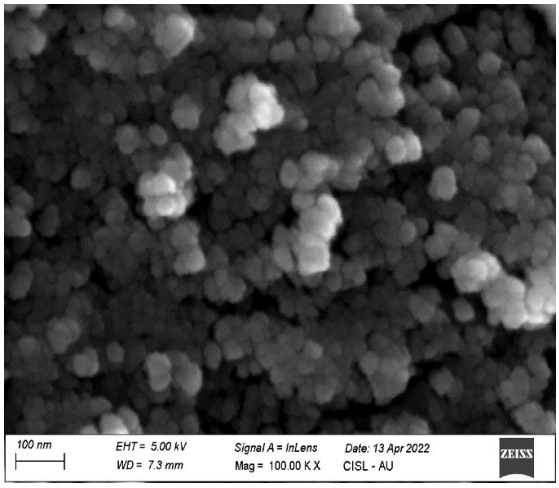


**(a)**

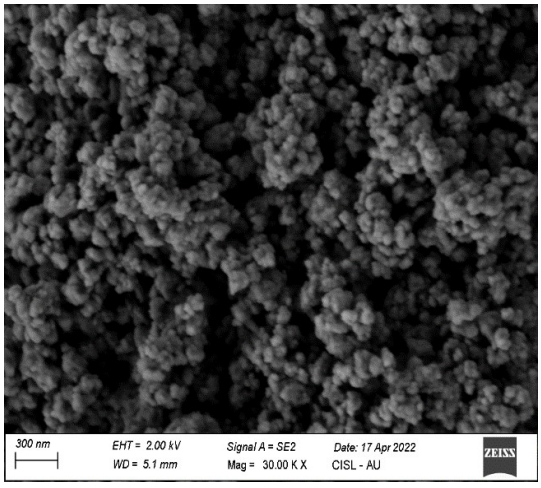


**(b)**

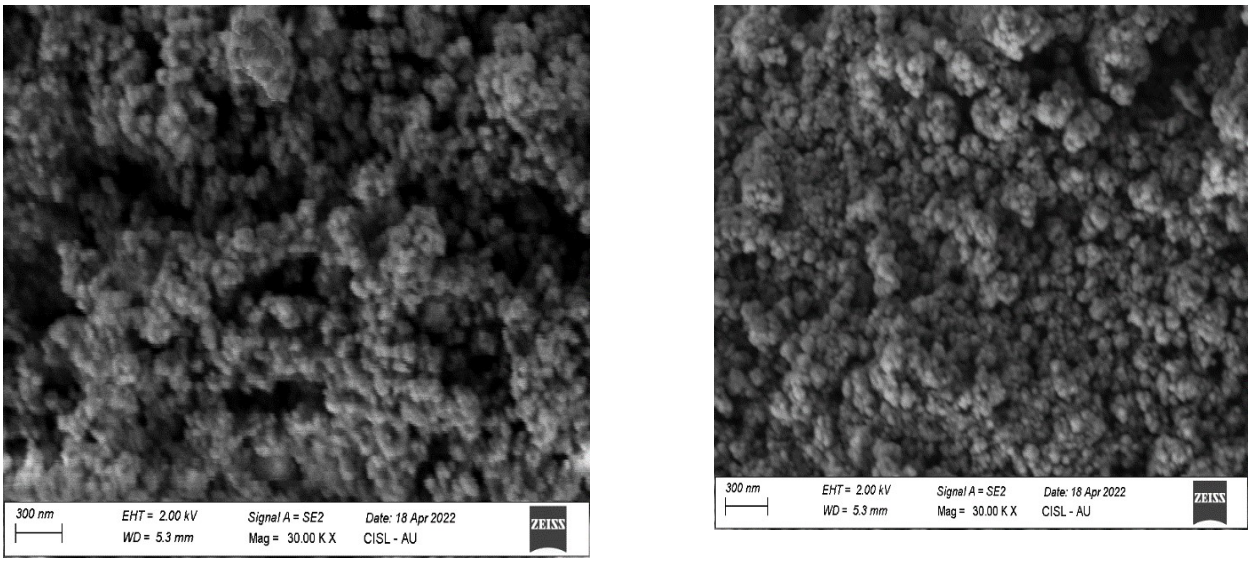


**(c)** **(d)**

**Figure 3.** FE-SEM images of **(a)** Indium sulfide; **(b)** Cu (0.01) g; **(c)** Cu (0.07) g; **(d)** Cu (0.1) doped Indium sulfide.

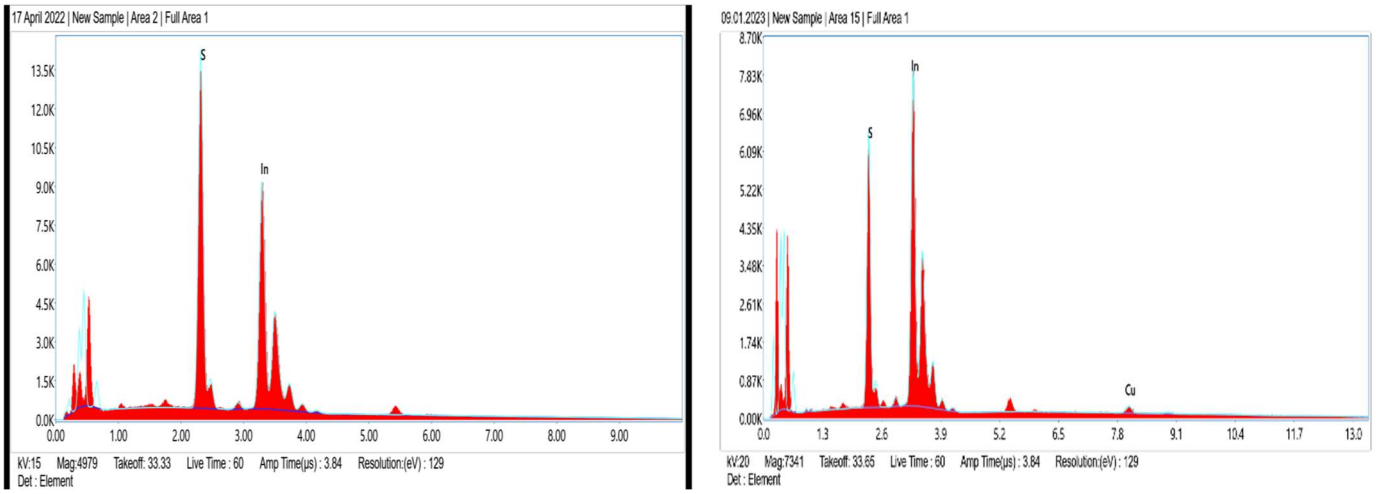


**(a)** **(b)**

**Figure 4.** EDX spectrum of pure **(a)** InS; **(b)** Cu-doped InS.

EDX analysis was used to determine the elemental contact of the synthesised samples [28–30]. The existence of In and S is confirmed by the EDX spectra of indium sulfide nanocrystals. **Figure 4a–b**. The presence of copper ions in the EDX spectra of copper-doped indium sulfide indicates that copper was successfully doped in InS. EDX spectra revealed that $CuCl_2$ doped InS had In, S, and Cu atomic percentages of 52.91, 43.17, and 03.93, respectively.

### 3.4. Optical absorption studies (UV-DRS)

To explore the optical quality, a UV-Visible diffuse reflectance spectra (UV-Vis DRS) investigation was carried out the light absorption capacity of the manufactured items. Reflectance is commonly defined as the ratio of radiant flux reflected to radiant flux incident. In the case of diffuse reflectance, the energy of the reflected radiation has been partially absorbed, transmitted, and scattered by a surface with no set angle

of reflection [31–34]. The UV-Vis DRS findings of pure indium sulfide and copper (0.01 g, 0.07 g, 0.1 g) doped indium sulfide nanocrystals recorded at 220 nm–1200 nm wavelength range are depicted in **Figure 5a–d.**

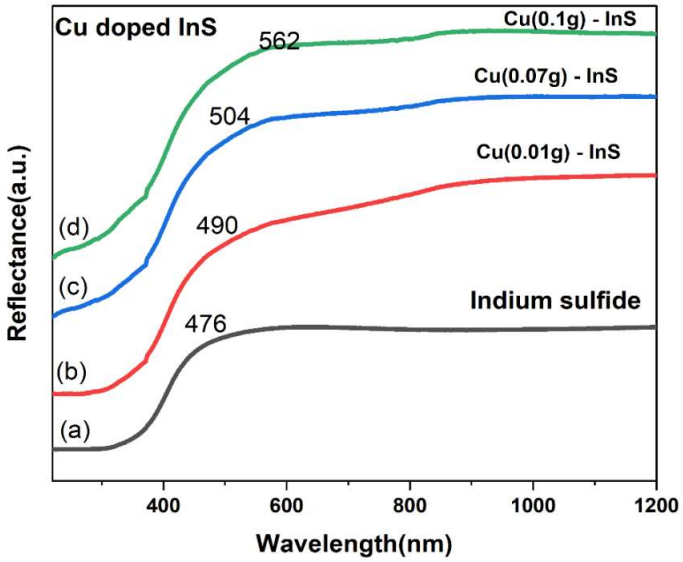


**Figure 5.** UV-Vis DRS of synthesized **(a)** Indium sulfide; **(b)** Cu (0.01) g; **(c)** Cu (0.07) g; **(d)** Cu (0.1) doped InS.

As shown in **Figure 5a–d** all the samples had optical activity in the UV range, with total reflectance ranging from 450 to 600 nm. The Kubelka—Munk function [35] can be used to calculate Eg.

$$[F(R)\,h]\,n = A\,(h - Eg),\ F(R) = (1-R)^2/2R)$$

where $F(R)$ is the Kubelka-Munk function for assistance and $R$ is the reflectance of the sample.

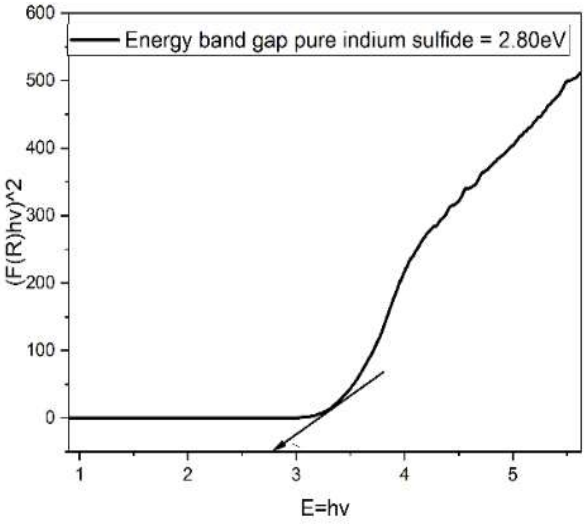


**(a)**

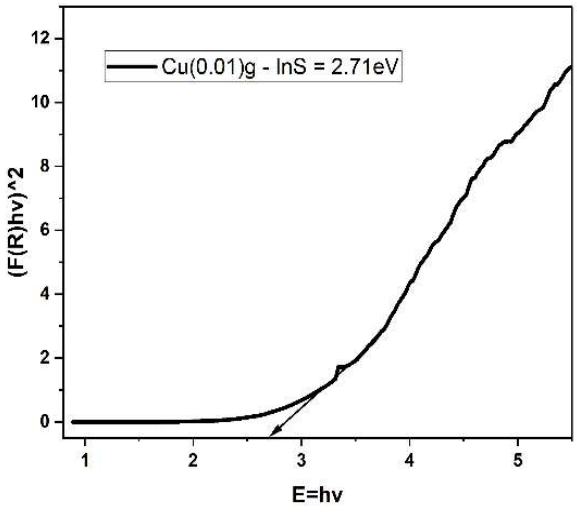


**(b)**

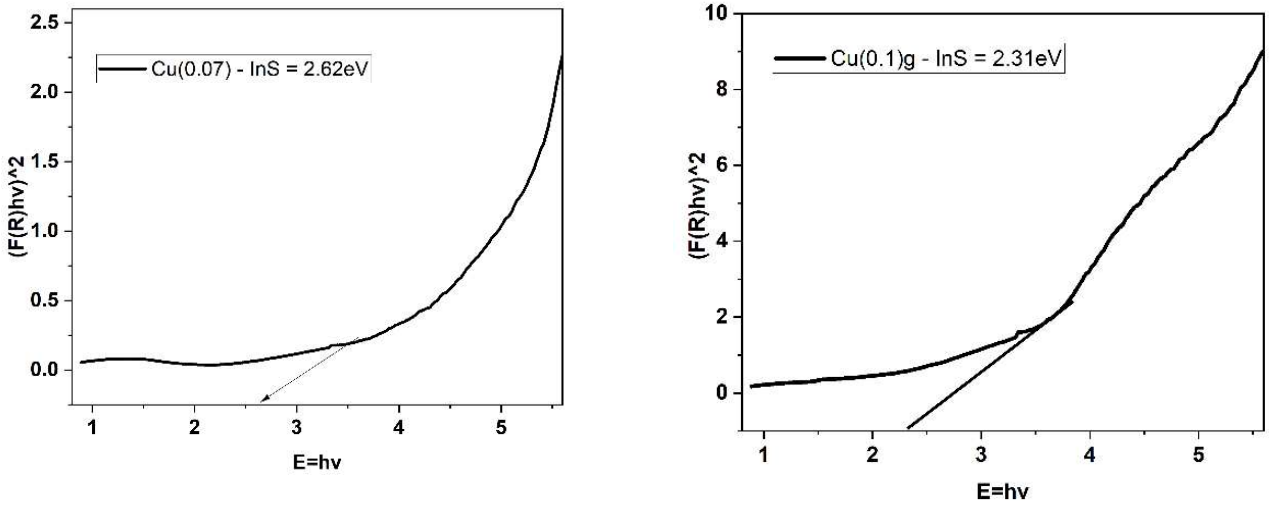


**(c)** **(d)**

**Figure 6.** Optical band gap spectra of **(a)** Indium sulfide; **(b)** Cu (0.01) g; **(c)** Cu (0.07) g; **(d)** Cu (0.1) doped InS NPs.

Extrapolating the linear component of the $(F(R)\ \mathrm{hv})^2$ curve versus the photo energy hv yields the optical band gap Eg. **Figure 6a–d** The figure shows that undoped indium sulfide has a band gap of 2.80 eV, whereas copper doped indium sulfide has estimated band gaps of 2.71 eV, 2.62 eV, and 2.31 eV. Doping indium sulfide with a low concentration of Cu (0.01) g resulted in a decrease in band gap due to a decrease in carrier concentration. Yet, as the concentration of copper (0.07 g and 0.1 g) increases, the value of the band gap falls. The band gap of nanocrystals appears to vary somewhat with doping concentration. This slight movement may be the result of a considerable surge in free-of-charge carriers. About copper ion doping and the subsequent shift of the Fermi level below the band edge. The mechanism for reducing the band gap is described below.

In terms of unstrained $E_g$, the band gap of a stressed $E_g$ can be defined as

$$E_g = E_c - E_v = -E_v = -(E_g^0 + \Delta E_v)$$

With reference the band gap position in stressed $E_g$ can be expressed unstrained $E_g$, unstressed position, the $E_v$ is change in valance band the position gives stresses, the negative $E_v$ value represents decrease of band gap. the positive $E_v$ value represents increase of band gap. The band gap stressed versus unstressed position there is change in strained and unstrained $E_g$.

Doping can generate the energy required to accommodate extended electrons by substituting copper ions for indium sites. These energy levels shrank, resulting in impurity-induced bands derived mostly from interactions between the Cu 2p and In 3d states. The impurity-of dopant induced bands now mix with the conductance band, narrowing the band gap [36–38].

## 3.5. Photoluminescence studies

The graphic displays the PL emission characteristics are recorded at a wavelength of 465 nm. The spectra (**Figure 7**) revealed the presence of two visible emission features at 465 and 528 nm. The appearance of an intense green peak at 528 nm and a

faint emission at 465 nm is due to intense intrinsic defects such as indium interstitials and vacancies.

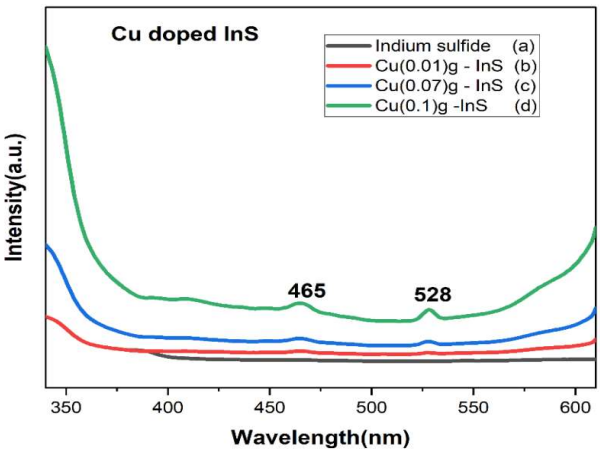


**Figure 7.** Photoluminescence spectra of synthesized **(a)** Indium sulfide; **(b)** Cu (0.01) g; **(c)** Cu (0.07) g; **(d)** Cu (0.1) doped InS NPs.

The presence of an emission band at 528 nm is caused by sulfur interstitials and lattice vacancies. Copper doping optimises the sulfur emission behaviour of indium sulfide. Doping can typically generate crystal structural strain in the host material. The strain produced may change the lattice's band length and band angle, resulting in the creation of numerous defect sites within the crystal structure. The visual emission intensity of all doped products is reduced when compared to indium sulfide that has not been doped for two reasons. One possibility is that the inherent weaknesses have been reduced. Despite the fact that doping increases the number of defect sites, the charge carriers can be kept from recombining in the defect sides. Copper (0.1 g) doped indium sulfide emits the most light, demonstrating its suitability for photocatalytic applications [39–41]. Furthermore, doping moves the red and blue emission peaks, while the green emission shifts substantially. These variations may be related to the differing depth levels of the problematic locations.

## 3.6. X-Ray photoelectron spectral analysis

The chemical composition determination and binding energy state of copper-doped indium sulfide are investigated using XPS. The graphic **Figure 8** illustrates the sample's intensity versus binding energy curves. The peaks obtained show the percentage of core-level electrons without collide at their initial energy level.

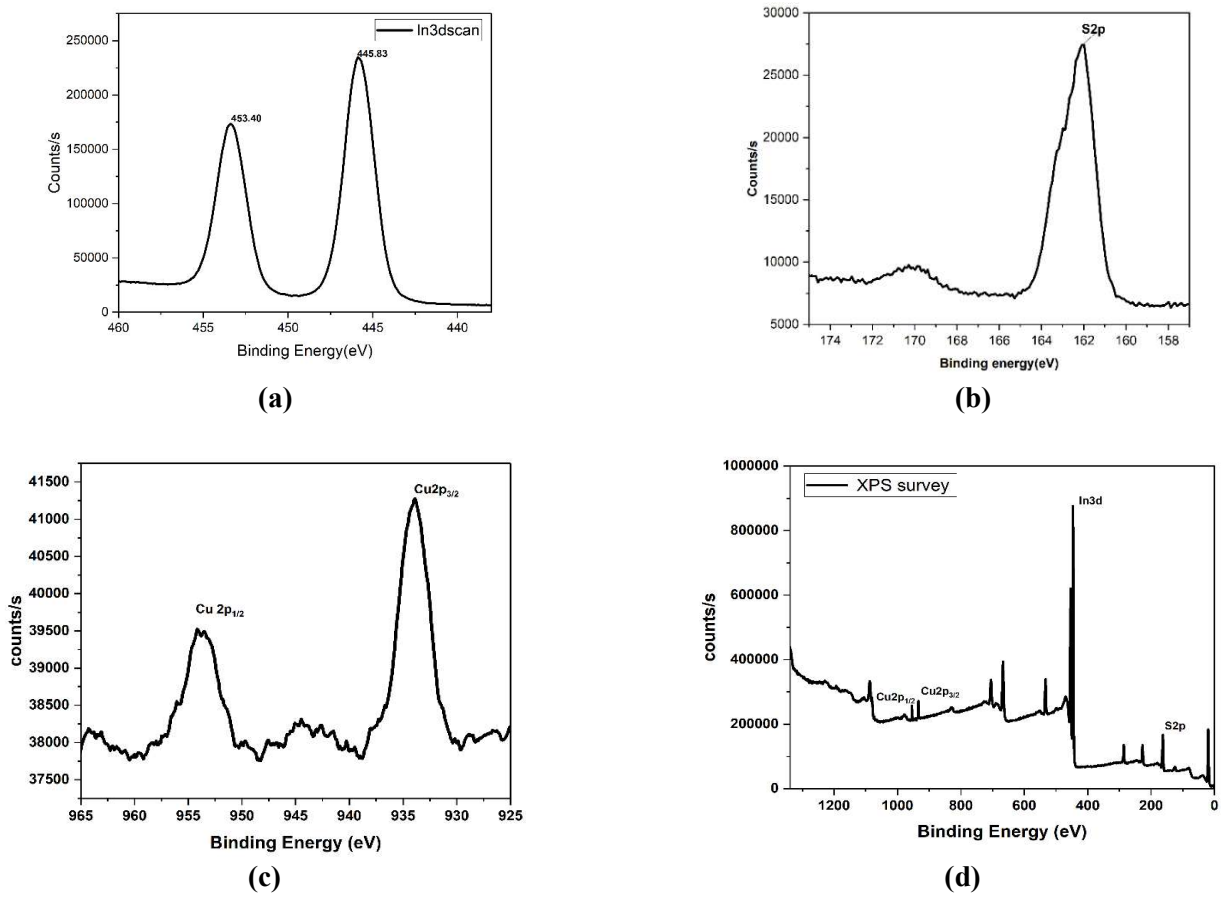


**Figure 8. (a)** In 3d; **(b)** S 2p; **(c)** Cu 2p binding energy spectrum of CuInS NPs; **(d)** XPS survey spectrum.

For core-level signals, the XPS notation is $Xn_j^l$, where $X$ is the element, $n$ is the principal quantum number ($n$ = 1, 2, 3), and l is the angular momentum quantum number designated as s, p, and f for l = 0, 1, 2, 3... ($n$ − 1). The quantum number of total angular momentum is represented by the letter $j$ ($j$ = l + $s$). The In 3d spectrum displays two significant peaks at 445.83 and 453.40 eV with a spin orbital splitting of 7.57 eV. These peaks match the binding energies of In $3d_{5/2}$ and In $3d_{3/2}$ perfectly, suggesting that In is present as $In^{3+}$. The S 2p and XPS areas of copper-doped indium sulfide are depicted in the figure. Because of the combination of sulfur ions and indium sulfide ions, the S 2p peaks are split into two at 162 eV and 170.55 eV. The Cu $2p_{3/2}$, Cu $2p_{1/2}$ spin orbital splitting of 19.93 eV suggests that copper ions in copper doped indium sulfide could have a valence of +2. As a result of the XPS results, $Cu^{2+}$ ions are successfully doped into indium sulfide lattices [42].

## 3.7. Photocatalytic studies

100 mL of a 0.03 mg/L methylene blue aqueous solution was mixed with 0.3 g of indium sulfide catalyst to compare the photocatalytic activity of indium sulfide and copper-doped indium sulfide against methylene blue. The sun was used as an irradiation source [43].

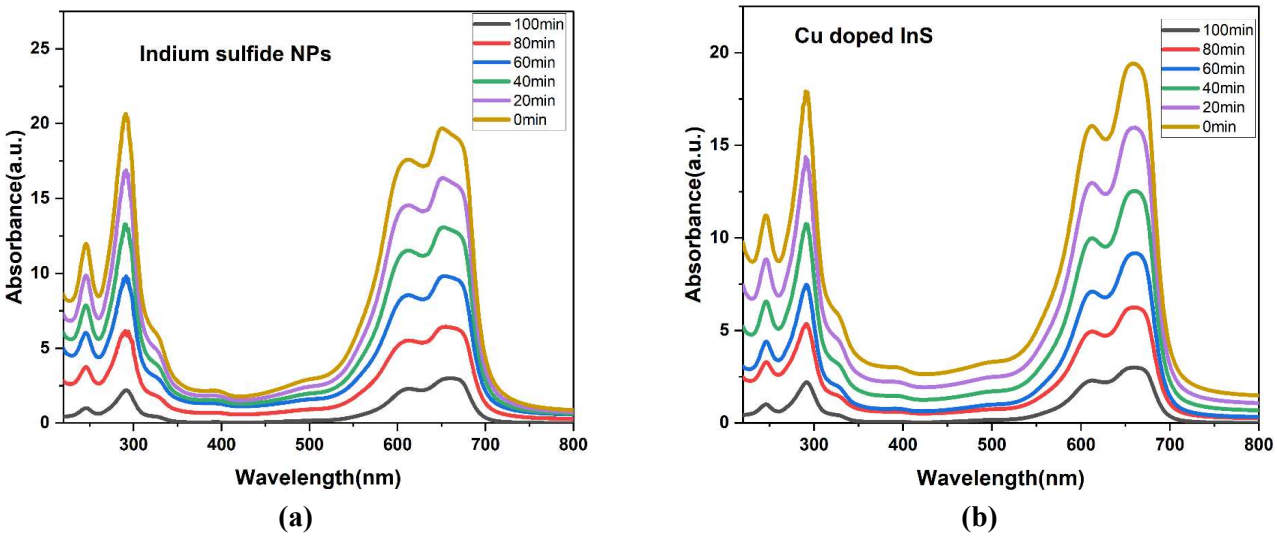


**Figure 9.** Absorption spectra of the MB solution presence of catalyst **(a)** InS; **(b)** Cu (0.1 g)—doped InS.

During light irradiation, 5mL of material was examined using a UV-Vis spectrophotometer at $P_{max}$ = 660 nm, and photodegradation was calculated using an equation.

$$X = (C_0 - C_t/C_0 \times 100\%)$$

$C_0$ = denotes the initial colourant concentration.

$C_t$ = dye concentration after irradiation within the specified time span

The electron-hole pair in reactive nature determines the photocatalytic activity of semiconductor nanoparticles. When exposed to light with a higher energy than the semiconductor's band gap reduce, one electron is excited to the conduction band, and another electron in the conduction band migrates to the lattice surface. The **Figure 9a–b** exhibit changes in the absorption pattern of methylene blue when exposed to sunlight for varied durations of time in the presence of indium sulfide and copper-doped indium sulfide.

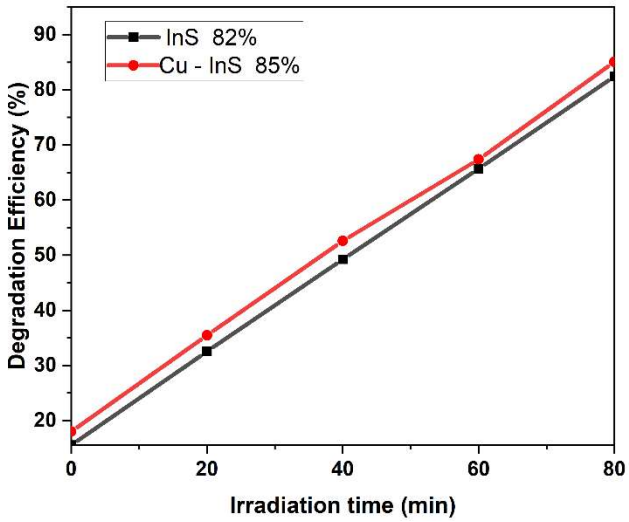


**Figure 10.** Percentage of photocatalytic degradation curves for different photocatalysts.

After 100 min of light irradiation, it is clear that indium sulfide destroyed 82% of the dye but not copper-doped indium sulfide. The degradation rate soared to 85 percent after 100 min of light exposure. This study (**Figure 10**) found that copper-doped indium sulfide has higher photocatalytic activity than pure indium sulfide. The rate constant values were calculated by using first order equation.in dye degradation reactions [44].

$$\ln (C_0/C) = kt$$

where $k$ represents the first order rate constant, $t$ is the time, and $C$ and $C_0$ are the dye concentrations before and after degradation.

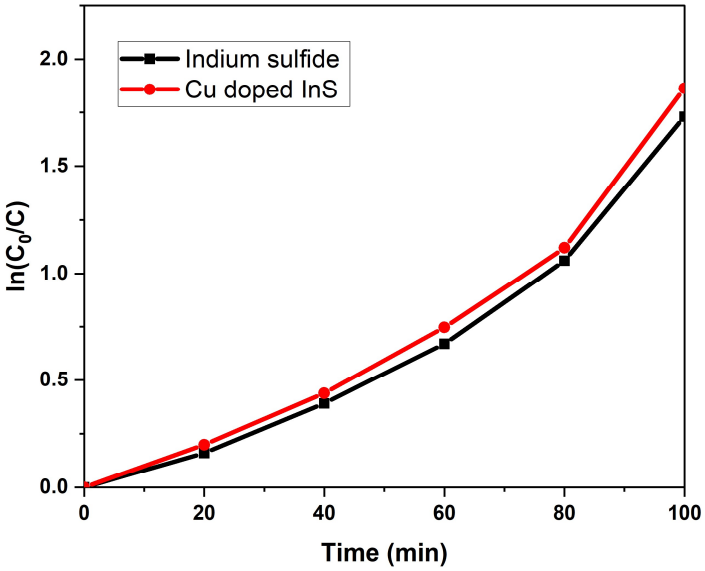


**Figure 11.** Pseudo-first-order reaction kinetic linear relationship curves for different photocatalysts.

For all samples, the **Figure 11** indicates a linear connection between ln $C_0/C$ and time, and rate constant values were computed based on the slope of the graph [45,46]. The rate constant of undoped indium sulfide was found to be on the order of 1.73051 $min^{-1}$, whereas the enhanced k value (1.863 $min^{-1}$) shows an increase in photocatalytic activity for copper-doped indium sulfide.

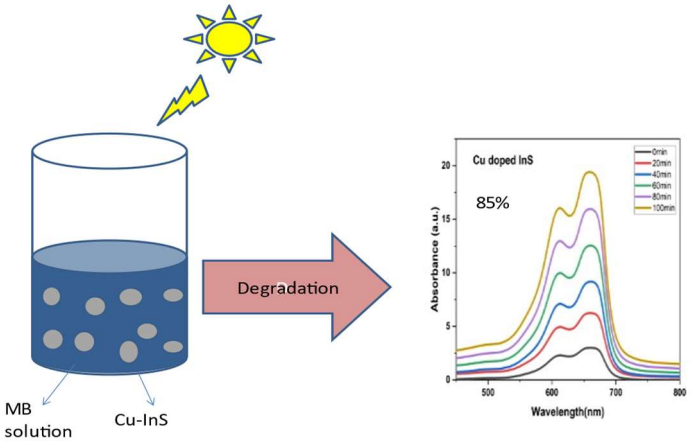


**Figure 12.** Photocatalytic mechanism of Cu (0.1g)-doped InS NPs.

The potential mechanism underlying the improved the photocatalytic activity of copper-doped indium sulfide is explained below **Figure12**.

When electrons from the valence band are exposed to light with an energy greater than the forbidden gap, they can make a quantum leap to the conduction band. Dopant $Cu^{2+}$ can occupy photogenerated electrons or holes, which are then transported to adsorbed oxygen, hydroxyl ions to produce super oxide radicals ($O^{2-}$) and hydroxide radicals ($OH^{-}$) [47]. This action inhibits electron-hole pair recombination and promotes the formation of free radicals, which are responsible for the breakdown of methylene blue. In this way, copper-doped indium sulfide exhibits enhanced activity in the breakdown of methylene blue dye.

### 3.8. Electrochemical studies (CV)

In 2 M aqueous KOH electrolytes, CV, GCD, and EIS measurements were performed on indium sulfide and copper-doped indium sulfide. The picture depicts CV curves of pure indium sulfide and copper doped indium sulfide electrodes at scan speeds of 5, 10, 15, 20, and 25 mV/s getting across the range of −0.0 eV to 0.4 eV.

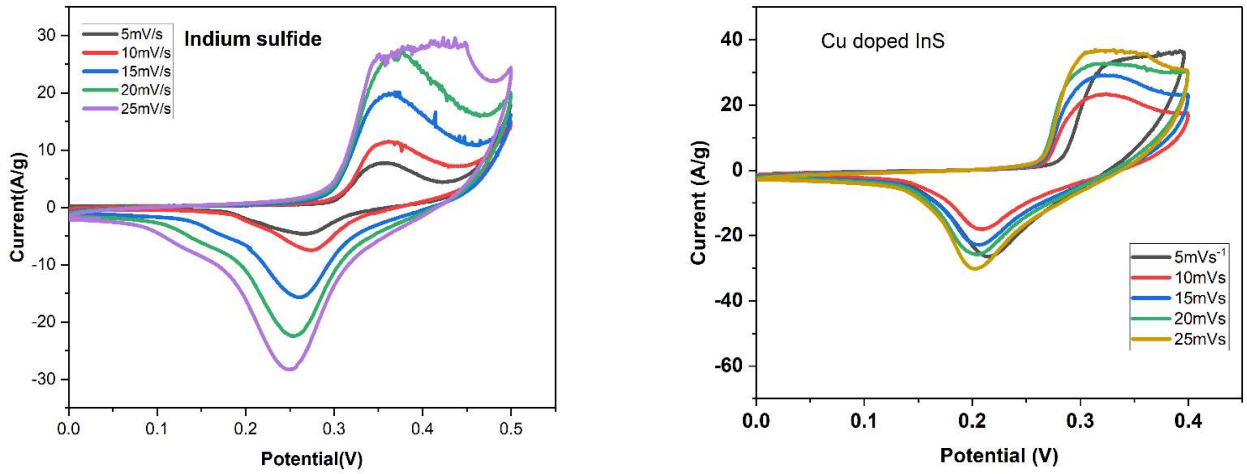


**(a)** **(b)**

**Figure 13.** (a) CV curve of Pure Indium sulfide; **(b)** CV curve of pure InS and Cu (0.1)g doped indium sulfide.

The CV curves of pure indium sulfide and copper-doped indium sulfide electrodes are roughly rectangular in shape and overlaid with a broad faradic curve spanning 0.00 to 0.35 eV. This **Figure 13** indicates that in pure indium sulfide and copper-doped indium sulfide electrodes, electrical double layer and faradic pseudo capacitance coexist. Furthermore, the *CV* curves behave similarly to the zero current line, revealed at each potential limit with a rapid current response to voltage.

$$C_{sp} = \frac{A}{k\Delta vm}$$

$C_{sp}$—Specific capacitance
$A$—Area of the quasi rectangular
$K$—Scan rate
$M$—mass of the active material
$\Delta v$—anodic and cathodic changes on each scanning.

**Table 2.** The specific capacitance of the Cu doped InS nanoparticles at the different scan rates.

| S. No. | Scan Rate (mV/s) | Specific Capacitance (Indium sulfide) (F/g) | Specific Capacitance (Cu-InS) (F/g) |
|---|---|---|---|
| 1. | 5 | 276 | 505 |
| 2. | 10 | 181 | 433 |
| 3. | 15 | 174 | 376 |
| 4. | 20 | 168 | 345 |
| 5. | 25 | 167 | 223 |

The results show that the copper-doped indium sulfide electrode outperforms the pure indium sulfide electrode in supercapacitor rate performance. The CV curves appear quasi-rectangular [48–50].

Curve deviation occurred moderately, as per **Table 2** when the scan rate was increased from 5 to 15 mV/s, but not when the scan rate was consistently increased to 20 and 25 mV/s. This can happen as a result of the electrode's overpotential and polarisation effect.

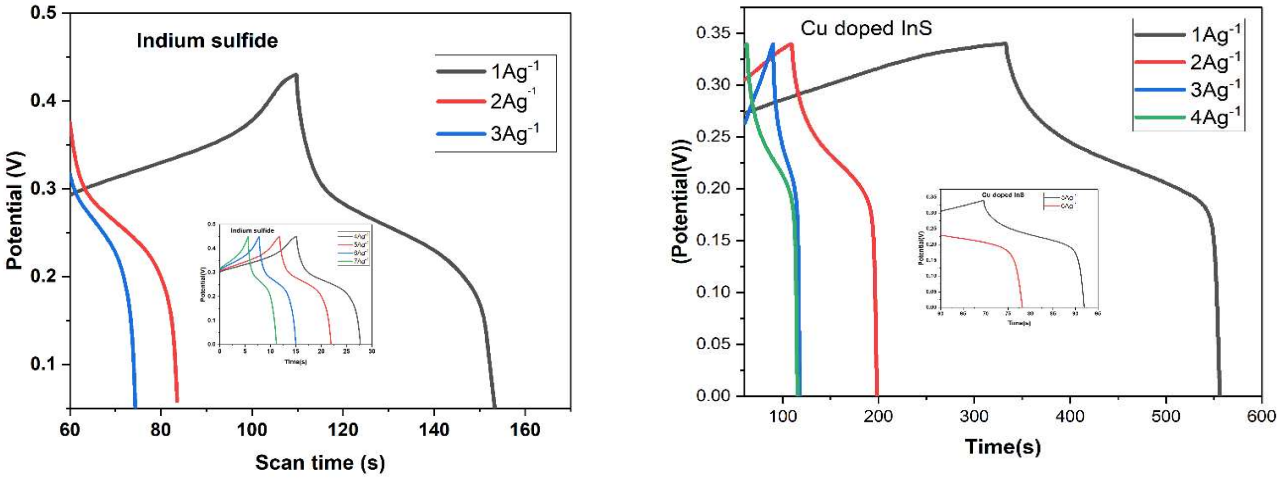


**(a)** **(b)**

**Figure 14. (a)** GCD curve of pure InS at different current densities; **(b)** GCD curve of pure InS and Cu (0.1) g doped indium sulfide at different current densities.

The graph (**Figure 14**) shows the galvanostic charging and discharging profiles of a copper-doped indium sulfide electrode with current densities of 1, 2, 3, 4, 5, 6, 7 $Ag^{-1}$ over a potential range of 0.0 to 0.4 V. The *C*s were calculated in accordance with

$$Cs = \frac{i\Delta t}{\Delta v m}$$

$\Delta t$—discharge time, $i$—discharge current, $\Delta v$—Potential change during discharge, $m$-mass of active material.

At 1, 2, 3, 4, 5, and 6 $Ag^{-1}$, the optimal value of the copper-doped indium sulfide electrode is 639, 505, 450, 394, 384, and 206 $Fg^{-1}$, respectively. Because of the increase in voltage drop and more or less insufficient use of electro-active material which are involved in the redox process, the Cs steadily declined as the current density grew, the values are presented in **Table 3**.

**Table 3.** The specific capacitance of the Cu doped InS nanoparticles at different current densities.

| S. No. | Current density (mA) | Specific Capacitance (Indium sulfide) (F/g) | Specific Capacitance (Cu-InS) (F/g) |
|---|---|---|---|
| 1. | 1 | 300 | 639 |
| 2. | 2 | 210 | 505 |
| 3. | 3 | 167 | 450 |
| 4. | 4 | 163 | 394 |
| 5. | 5 | 156 | 384 |
| 6. | 6 | 127 | 206 |
| 7. | 7 | 124 | - |

Response as current density increases. The copper doped indium sulfide electrode, on the other hand, exhibits exceptional specific capacitance at all current densities and excellent rate capability because the zero-dimensional nanostructure of copper doped indium sulfide enables rapid transport of electrolyte ions, which is conducive to the development of rate capability in electrodes.

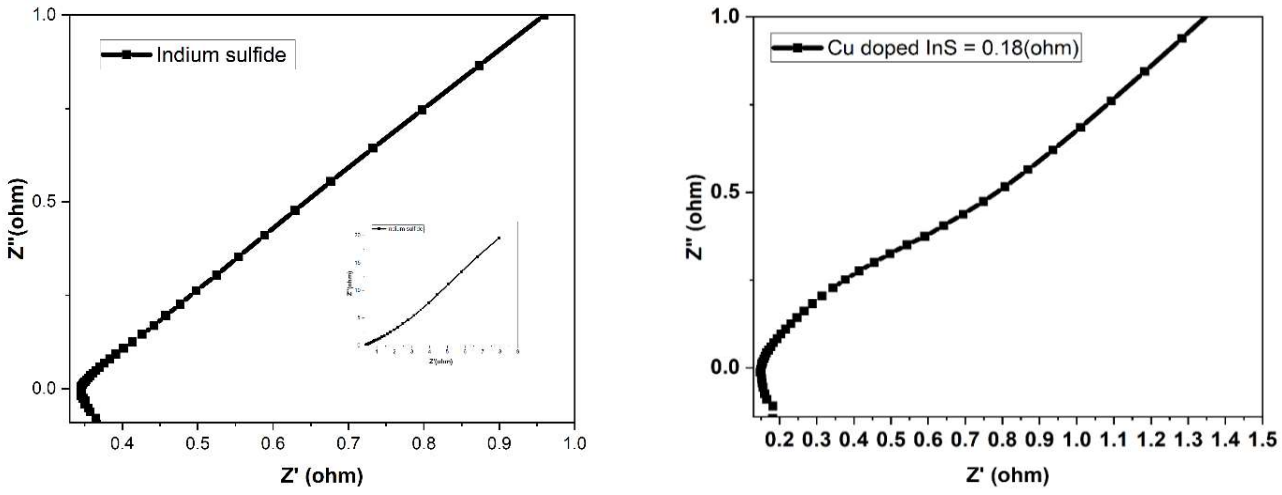


**(a)** **(b)**

**Figure 15. (a)** Electrochemical impedance spectra of pure InS; **(b)** Electrochemical impedance spectra of pure InS and Cu (0.1 g) doped InS.

The electrochemical behaviour of a copper-implanted indium sulfide electrode. Using an open circuit potential, electrochemical impedance study was performed in the frequency range of 100 mHz to 100 kHz. The Nyquist curve of the copper-doped indium sulfide electrode is shown in **Figure 15 a–b**. A single semicircle region in the high frequency zone corresponds to the apparent resistance during charge transfer at the solid sulfide electrolyte interface, but a practically straight line in the low frequency zone shows electrolyte ionic diffusion. According to the electrochemical impedance analysis, the copper-doped indium sulfide electrode is suitable for supercapacitor applications [51].

## 4. Conclusion

The easy hydrothermal procedure provides a simple and efficient method for producing pure indium sulfide and copper-doped indium sulfide nanoparticles (NPs).

Both pure and Cu-doped Indium sulfide nanoparticles (NPs) were polycrystalline with an orthorhombic structure and somewhat displaced due to an increase in volume with increasing Cu doping concentration, according to XRD data. Cu-doped InS nanoparticles had an orthorhombic BCC form with a particle size range of 14 to 20 nm. The band gap energy level of the manufactured InS nanoparticles with dopant $Cu^{2+}$ is raised due to the quantum confinement effect. In PL data, Cu-doped InS nanoparticles showed increased visible emissions. Photocatalytic tests demonstrated that doped NPs increased the MB dye's photodegradation percentage, suggesting a unique way to treating water contamination and environmental pollution. The Cu-doped InS electrode outperformed pure indium sulfide in electrochemical performance, with a maximum specific capacitance of 639 $Fg^{-1}$. According to the findings, the cu-doped indium sulfide nanoparticles produced might be used in MB photocatalytic degradation and electrochemical performance.

**Author contributions:** Conceptualization, investigation, original draft preparation, reviewing and editing, LMK; supervision, GD and RPS. All authors have read and agreed to the published version of the manuscript.

**Conflict of interest:** The authors declare no conflict of interest.

## References


1. Motaung MP, Onwudiwe DC, Wei L, et al. CuS, In2S3 and CuInS2 nanoparticles by microwave-assisted solvothermal route and their electrochemical studies. Journal of Physics and Chemistry of Solids. 2022; 160: 110319. doi: 10.1016/j.jpcs.2021.110319
2. Soni V, Raizada P, Kumar A, et al. Indium sulfide-based photocatalysts for hydrogen production and water cleaning: a review. Environmental Chemistry Letters. 2021; 19(2): 1065−1095. doi: 10.1007/s10311-020-01148-w
3. Sanchez-Tizapa M, Sosa-Muñiz MC, Flores-Martínez M, et al. Electrical characterization of electrodeposited indium sulfide thin films by electrochemical impedance spectroscopy and electrical force microscopy. Materials Science in Semiconductor Processing. 2020; 120: 105248. doi: 10.1016/j.mssp.2020.105248
4. Sawant JP, Bhujbal PK, et al. Copper Indium Disulfide Thin Films: Electrochemical Deposition and Properties. ES Materials & Manufacturing; 2022. doi: 10.30919/esmm5f629
5. Kennedy A, Ganesan H, Marnadu R, et al. An effect of metal ions (Cu, Mn) doping on the structural, morphological, optical, photoluminescence, electrical and photocatalytic properties of In2S3 nanoparticles. Optical Materials. 2022; 124: 111769. doi: 10.1016/j.optmat.2021.111769
6. Vakalopoulou E, Rath T, Warchomicka FG, et al. Honeycomb-structured copper indium sulfide thin films obtainedviaa nanosphere colloidal lithography method. Materials Advances. 2022; 3(6): 2884-2895. doi: 10.1039/d2ma00004k
7. Suthakaran S, Dhanapandian S, Krishnakumar N, et al. Surfactants assisted SnO2 nanoparticles synthesized by a hydrothermal approach and potential applications in water purification and energy conversion. Journal of Materials Science: Materials in Electronics. 2019; 30(14): 13174−13190. doi: 10.1007/s10854-019-01681-7
8. Yan D, Lim YV, Wang G, et al. Unlocking Rapid and Robust Sodium Storage Performance of Zinc-Based Sulfide via Indium Incorporation. ACS Nano. 2021; 15(5): 8507-8516. doi: 10.1021/acsnano.1c00131
9. Farzi M, Moradi M, Hajati S, et al. Synthesis of rod-like ternary Cu(Cd)-In-S and quaternary Cu-Cd-In-S by controlled ion exchange of MIL-68(In) derived indium sulfide for high energy-storage capacitor. Synthetic Metals. 2021; 278: 116815. doi: 10.1016/j.synthmet.2021.116815
10. Kennedy A, Ganesan H, Govindaraj T, et al. Effect of Metal (Cu, Mn) Doping on the Structural, Morphological, Optical, Photoluminescence, Electrical and Photocatalytic Properties of In2s3 Nanoparticles. https://doi.org/10.21203/rs.3.rs-588347/v1.
11. Ethiraj AS, Uttam P, KV, et al. Photocatalytic performance of a novel semiconductor nanocatalyst: Copper doped nickel oxide for phenol degradation. Materials Chemistry and Physics. 2020; 242: 122520. doi:

10.1016/j.matchemphys.2019.122520
12. Chen YX, Li F, Wang W, et al. Optimization of thermoelectric properties achieved in Cu doped β-In2S3 bulks. Journal of Alloys and Compounds. 2019; 782: 641-647. doi: 10.1016/j.jallcom.2018.12.138
13. Jiao M, Huang X, Ma L, et al. Biocompatible off-stoichiometric copper indium sulfide quantum dots with tunable near-infrared emission via aqueous based synthesis. Chemical Communications. 2019; 55(100): 15053−15056. doi: 10.1039/c9cc07674c
14. Higashimoto S, Nakase T, Mukai S, et al. Copper-indium-sulfide colloids on quantum dot sensitized TiO2 solar cell: Effects of capping with mercapto-acid linker molecules. Journal of Colloid and Interface Science. 2019; 535: 176−181. doi: 10.1016/j.jcis.2018.09.092
15. Kumar S, Yadav N, Kumar P, et al. Design and Comparative Studies of Z-Scheme and Type II Based Heterostructures of NaNbO3/CuInS2/In2S3 for Efficient Photoelectrochemical Applications. Inorganic Chemistry. 2018; 57(24): 15112−15122. doi: 10.1021/acs.inorgchem.8b02264
16. Mousavi-Kamazani M. A green and simple hydrothermal approach to synthesize needle-like CuInS2 nanostructures for solar cells. Journal of Materials Science: Materials in Electronics. 2018; 29(18): 16050−16056. doi: 10.1007/s10854-018-9693-9
17. Sharma RK, Chouryal YN, Nigam S, et al. Tuning the Crystal Phase and Morphology of the Photoluminescent Indium Sulphide Nanocrystals and Their Adsorption-Based Catalytic and Photocatalytic Applications. ChemistrySelect. 2018; 3(28): 8171-8182. doi: 10.1002/slct.201801006
18. Aydin E, Demirci Sankir N. AZO/metal/AZO transparent conductive oxide thin films for spray pyrolyzed copper indium sulfide based solar cells. Thin Solid Films. 2018; 653: 29-36. doi: 10.1016/j.tsf.2018.03.012
19. Bi K, Sui N, Wang Y, et al. Temperature-dependent charge carrier dynamics investigation of heterostructured Cu2S-In2S3 nanocrystals films using injected charge extraction by linearly increasing voltage. Applied Physics Letters. 2017; 110(8). doi: 10.1063/1.4977000
20. Silambarasan M, Ramesh PS, Geetha D, et al. A report on 1D MgCo2O4 with enhanced structural, morphological and electrochemical properties. Journal of Materials Science: Materials in Electronics. 2017; 28(9): 6880-6888. doi: 10.1007/s10854-017-6388-6
21. Li M, Zhao R, Su Y, et al. Synthesis of CuInS2 nanowire arrays via solution transformation of Cu2S self-template for enhanced photoelectrochemical performance. Applied Catalysis B: Environmental. 2017; 203: 715-724. doi: 10.1016/j.apcatb.2016.10.051
22. Frank A, Wochnik AS, Bein T, et al. A biomolecule-assisted, cost-efficient route for growing tunable CuInS2 films for green energy application. RSC Advances. 2017; 7(33): 20219-20230. doi: 10.1039/c6ra27294k
23. Esmaili P, Kangarlou H, Savaloni H, et al. Structural, optical and electronic properties of indium sulfide compositions under influence of copper impurity produced by chemical method. Results in Physics. 2017; 7: 3380-3389. doi: 10.1016/j.rinp.2017.08.062
24. Zhao Y, Luo F, Zhuang M, et al. Synthesis of nanostructured CuInS2 thin films and their application in dye-sensitized solar cells. Applied Physics A. 2016; 122(3). doi: 10.1007/s00339-016-9718-2
25. Zhao X, Huang Y, Corrigan JF. Facile Preparation of Wurtzite CuInE2 (E = S, Se) Nanoparticles Under Solvothermal Conditions. Inorganic Chemistry. 2016; 55(20): 10810−10817. doi: 10.1021/acs.inorgchem.6b02177
26. Yang W, Oh Y, Kim J, et al. Photoelectrochemical Properties of Vertically Aligned CuInS2 Nanorod Arrays Prepared via Template-Assisted Growth and Transfer. ACS Applied Materials & Interfaces. 2015; 8(1): 425-431. doi: 10.1021/acsami.5b09241
27. Tamil Illakkiya J, Usha Rajalakshmi P, Oommen R. Enhanced optoelectronic and photoelectrochemical characteristics of nebulised spray pyrolysed 'Cu' rich CuInS2 thin film. Materials Science in Semiconductor Processing. 2016; 49: 84-91. doi: 10.1016/j.mssp.2016.03.027
28. Leach ADP, Macdonald JE. Optoelectronic Properties of CuInS2 Nanocrystals and Their Origin. The Journal of Physical Chemistry Letters. 2016; 7(3): 572-583. doi: 10.1021/acs.jpclett.5b02211
29. Dunst S, Rath T, Reichmann A, et al. A comparison of copper indium sulfide-polymer nanocomposite solar cells in inverted and regular device architecture. Synthetic Metals. 2016; 222: 115−123. doi: 10.1016/j.synthmet.2016.04.003
30. Chen Y, Qin Z, Guo X, et al. One-step hydrothermal synthesis of (CuIn)0.2Zn1.6S2 hollow sub-microspheres for efficient visible-light-driven photocatalytic hydrogen generation. International Journal of Hydrogen Energy. 2016; 41(3): 1524−1534. doi: 10.1016/j.ijhydene.2015.11.087

31. Zheng Z, Yu J, Cheng S, et al. Investigation of structural, optical and electrical properties of Cu doped β-In2S3 thin films. Journal of Materials Science: Materials in Electronics. 2016; 27(6): 5810-5817. doi: 10.1007/s10854-016-4496-3
32. Rajendar V, Dayakar T, Satish B, et al. Synthesis and Characterization of Cuins2 Nanoparticles as Potential Candidates for Photocatalyst and Photovoltaic Materials Synthesis and Characterization of CuInS2 Nanoparticles as Potential Candidates for Photocatalyst and Photovoltaic Materials. Chalcogenide Letters. 2016; 13(10).
33. Mahanthappa M, Yellappa S, Kottam N, et al. Sensitive determination of caffeine by copper sulphide nanoparticles modified carbon paste electrode. Sensors and Actuators A: Physical. 2016; 248: 104−113. doi: 10.1016/j.sna.2016.07.013
34. Krishnakanth R, Jayakumar G, Albert Irudayaraj A, et al. Structural and Magnetic Properties of NiO and Fe-doped NiO Nanoparticles Synthesized by Chemical Co-precipitation Method. Materials Today: Proceedings. 2016; 3(6): 1370−1377. doi: 10.1016/j.matpr.2016.04.017
35. Baneto M, Enesca A, Mihoreanu C, et al. Effects of the growth temperature on the properties of spray deposited CuInS2 thin films for photovoltaic applications. Ceramics International. 2015; 41(3): 4742-4749. doi: 10.1016/j.ceramint.2014.12.023
36. Shanmugam N, Suthakaran S, Kannadasan N, et al. Synthesis and Characterization of Te Doped ZnO Nanosheets for Photocatalytic Application. Journal of Heterocyclics. 2015: 15-20. doi: 10.33805/2639-6734.105
37. Jrad A, Ben Nasr T, Turki-Kamoun N. Study of structural, optical and photoluminescence properties of indium-doped zinc sulfide thin films for optoelectronic applications. Optical Materials. 2015; 50: 128−133. doi: 10.1016/j.optmat.2015.10.011
38. Xue B, Xu F, Wang B, et al. Shape-controlled synthesis of β-In2S3nanocrystals and their lithium storage properties. CrystEngComm. 2016; 18(2): 250-256. doi: 10.1039/c5ce01955a
39. Gannouni M, Assaker IB, Chtourou R. Experimental investigation of the effect of indium content on the CuIn5S8 electrodes using electrochemical impedance spectroscopy. Materials Research Bulletin. 2015; 61: 519-527. doi: 10.1016/j.materresbull.2014.10.070
40. Xie BB, Hu BB, Jiang LF, et al. The phase transformation of CuInS2 from chalcopyrite to wurtzite. Nanoscale Research Letters. 2015; 10(1). doi: 10.1186/s11671-015-0800-z
41. Paquin F, Rivnay J, Salleo A, et al. Multi-phase microstructures drive exciton dissociation in neat semicrystalline polymeric semiconductors. Journal of Materials Chemistry C. 2015; 3(41): 10715−10722. doi: 10.1039/c5tc02043c
42. Park JC, Nam YS. Controlling surface defects of non-stoichiometric copper-indium-sulfide quantum dots. Journal of Colloid and Interface Science. 2015; 460: 173−180. doi: 10.1016/j.jcis.2015.08.037
43. Dhanya AC, Preetha KC, Deepa K, et al. Crystalline Indium Sulphide thin film by photo accelerated deposition technique. IOP Conference Series: Materials Science and Engineering. 2015; 73: 012009. doi: 10.1088/1757-899x/73/1/012009
44. Gao W, Liu W, Leng Y, et al. In2S3 nanomaterial as a broadband spectrum photocatalyst to display significant activity. Applied Catalysis B: Environmental. 2015; 176−177: 83-90. doi: 10.1016/j.apcatb.2015.03.048
45. Yin HY, Tang JH, Yan CJ, et al. Facile Preparation of the Single Crystalline In2S3 Nanosheets with Highly Efficient Photocatalytic Activity. Advanced Materials Research. 2013; 834-836: 8−11. doi: 10.4028/www.scientific.net/amr.834-836.8
46. Lugo-Loredo S, Peña-Méndez Y, Calixto-Rodriguez M, et al. Indium sulfide thin films as window layer in chemically deposited solar cells. Thin Solid Films. 2014; 550: 110−113. doi: 10.1016/j.tsf.2013.10.115
47. Aslan F, Adam G, Stadler P, et al. Sol–gel derived In 2 S 3 buffer layers for inverted organic photovoltaic cells. Solar Energy. 2014; 108: 230-237. doi: 10.1016/j.solener.2014.07.011
48. Shang X, Wang Z, Li M, et al. A numerical simulation study of CuInS2 solar cells. Thin Solid Films. 2014; 550: 649-653. doi: 10.1016/j.tsf.2013.10.047
49. Amiri O, Salavati-Niasari M, Sabet M, et al. Sonochemical Method for Preparation of Copper Indium Sulfide Nanoparticles and their Application for Solar Cell. Combinatorial Chemistry & High Throughput Screening. 2014; 17(2): 183−189. doi: 10.2174/1386207311301010001
50. Yan C, Liu F, Song N, et al. Band alignments of different buffer layers (CdS, Zn(O,S), and In2S3) on Cu2ZnSnS4. Applied Physics Letters. 2014; 104(17). doi: 10.1063/1.4873715
51. Sun J, Chen G, Feng Y, et al. Ag/Cu co-doped ZnS–In2S3solid solutions: facile synthesis, theoretical calculations and enhanced photocatalytic activity. RSC Adv. 2014; 4(84): 44466-44471. doi: 10.1039/c4ra05960c